ACS Photonics

Article

pubs.acs.org/journal/apchd5

Tunable Raman Selectivity via Randomization of a Rectangular Pattern of Nanodisks

Yoshiaki Nishijima,*[,†] Jacob B. Khurgin,[‡] Lorenzo Rosa,[§,⊥] Hideki Fujiwara,[∥] and Saulius Juodkazis[§,⊥]

[†]Department of Electrical and Computer Engineering, Graduate School of Engineering, Yokohama National University, 79-5 Tokiwadai, Hodogaya-ku, Yokohama 240-8501, Japan

[‡]Department of Electrical and Computer Engineering, Johns Hopkins University, Baltimore, Maryland 21218, United States

[§]Centre for Micro-Photonics, Faculty of Engineering and Industrial Sciences, Swinburne University of Technology, Hawthorn, VIC 3122, Australia

[⊥]Melbourne Centre for Nanofabrication (MCN), Australian National Fabrication Facility, Clayton, VIC 3168, Australia

[∥]Research Institute for Electronic Science, Hokkaido University, North 21 West 10, Kita-ku, Sapporo, Hokkaido, Japan

ABSTRACT: We show that randomization of a nanodisk array on a rectangular lattice can be used to spectrally tune the surface-enhanced Raman scattering (SERS) intensity and to control the field enhancement. The spectral selectivity of the Raman modes exhibits a nonlinear dependence on the extinction. Randomization of the rectangular pattern brings a favorable increase of SERS intensity via a reduced selectivity and extinction changes at the Stokes band. The extinction dependence for two polarizations on the spacing in the rectangular array is demonstrated. For a given polarization, the extinction strength depends primarily on the spacing between the nanodisks in the orthogonal direction. Such randomization and polarization control of SERS increases the versatility, e.g., all-optical control, of this important sensing tool.

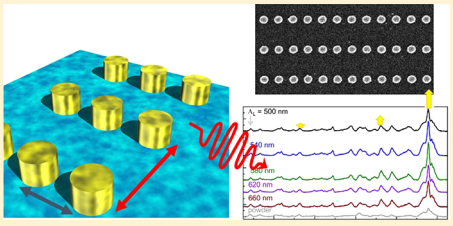

KEYWORDS: *nanomaterials, surface plasmons, plasmonics, multiple scattering, nanostructure fabrication, subwavelength structures, nanostructures*

Surface-enhanced Raman scattering (SERS)[1] is a promising method for highly sensitive detection of a small number of molecules due to strong enhancement of the local light field intensity, $|E|^2 \approx 10^2-10^4$, in close proximity to nanoparticles[2−5] and even reaching single-molecular detection levels with 10^{11} enhancements at the hot-spots between two nanoparticles.[6] However, SERS of complex molecules gives a large number of molecular vibrations, with the total number of $3N - 6$ for nonlinearly shaped molecules (including transitions of the IR absorption and Raman modes), where N is the number of atoms; hence, the spectral SERS signatures become complicated with an increasing number of atoms, and even more so for actual biosamples such as proteins, DNA, and cells.[7−9] Therefore, achieving a high selectivity in the excitation of molecular vibrational modes is very important for sensing applications,[10,11] especially in the detection of explosives,[12] environmental pollutants such as Hg ions,[13] biomaterials,[14−17] (photo-) catalysis,[18,19] immunoassay,[20] and in situ detection in the microfluidics.[21,22]

Typically, selective detection of hazardous materials (cations coming from heavy metals such as Hg, Cd, As, anions from NO_3^-, SO_4^{2-}) has been done by controlling the chemical components such as crown ethers and cyclodextrin molecules with absorption/fluorescence spectroscopy on the surface of metals. In addition to EM field enhancement, the SERS signal can be further enhanced by the resonance between the excitation and Stokes frequencies and the electronic energy levels in the molecule.[23−26] Since different molecules have different electronic structures, controlling the spectral position of the peak of EM enhancement can provide highly desired selectivity to SERS.

One promising approach is to use complex nanoparticles where interaction and hybridization of plasmonic modes brings about Fano resonances[27−29] and dark modes,[30] which are spectrally narrow and whose spectral position can be engineered via the particles' geometry. It has been demonstrated that rectangular arrays with two different periodicities can provide control over the spectral behavior of plasmon resonances.[31,32] This was achieved via coupling of plasmons and light scattering in the two perpendicular in-plane directions. Recently, coupling between nanoparticle arrays via hybridized modes distinct from near- and far-field mediated radiation is revealed[33] and explained via plasmonic Young interference. Control of such coupling could be useful to tune selectivity in SERS. However, rectangular patterns have a low density of nanoparticles and relatively small total enhancement factors. Therefore, a method to further enhance SERS intensity is required.

We have recently demonstrated that plasmon resonances can be controlled spectrally via randomization of patterns,[34,35] and this causes an increase in the SERS intensity by a factor of 4.[36]

Received: June 23, 2014
Published: September 22, 2014

The randomization also suppresses the diffraction pattern in the Raman scattered radiation. Here we demonstrate a practical way for controlling the surface plasmon resonances by varying the ratio of the periods between nanodisks on a rectangular lattice. Surprisingly, the extinction of one polarization depends primarily on the spacing between the nanodisks in the orthogonal direction. The total SERS intensity is enhanced by the randomization of the rectangular array. We discuss the trade-off relationship between SERS selectivity and intensity.

SAMPLES AND METHODS

Samples of Au nanodisks on a cover glass were fabricated by electron beam lithography, Au sputtering, and lift-off for the 150 × 150 μm^2 areas.[34] Figure 1a shows the scanning electron microscopy (SEM) image of a rectangular lattice pattern of nanodisks of 180 nm diameter and 50 nm height, whose elementary cell pitch along the x-axis is Λ_S = 300 nm and the pitch along the y-axis is Λ_L = 680 nm (the designations stand for "short" and "long"); the spacing is also apparent in the fast Fourier transform (FFT) of the lattice shown in Figure 1b.

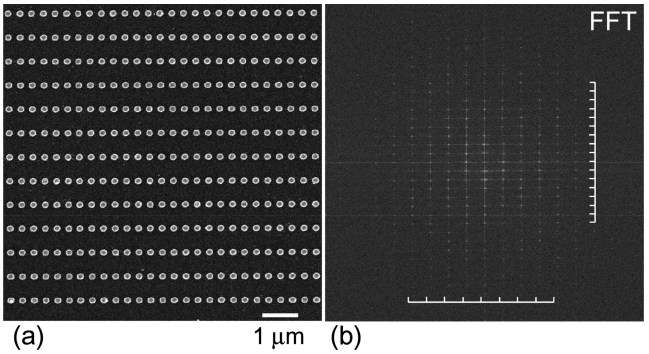

Figure 1. (a) SEM and (b) FFT images of the rectangular lattice of Au nanodisks on a cover glass; the x- and y-periods of the elementary cell are Λ_S = 300 nm (short pitch) and Λ_L = 680 nm (long pitch), respectively.

The laser dye IR-26 (Exciton) was used for SERS measurements on a Raman-dedicated inVIA (Renishaw) microscope. Samples were immersed into a dichloromethane (10^{-4} M) solution of the dye and incubated for 10 h. After that, samples were rinsed in pure dichloromethane and then in methanol. SERS measurements were carried out on dried samples. The IR-26 is chemisorbed on gold and makes a permanent bond via its sulfur atom. Extinction spectra were measured by microscopic spectroscopy using an IX-71 inverse microscope (Olympus) with a 40× objective lens with a numerical aperture (NA) of 0.75. The confocal pinhole size was 1 mm in diameter, which corresponds to a 1 mm/40 ≃ 25 μm spot on the sample. SERS was measured using a Raman microscope with a 20× objective lens focusing on a linear spot of 100 × 5 μm^2 cross-section on the sample. The excitation wavelength of the semiconductor laser was λ_l = 785 nm, and the acquisition time was ∼10 s.

RESULTS AND DISCUSSION

Figure 2 shows the optical extinction spectra of the rectangular lattice nanodisk arrays under nonpolarized light (black line) and two perpendicular linear polarizations aligned with the short (pol.-P_S) and long (pol.-P_L) pitch, respectively. The spacing Λ_S was fixed to 300 nm for all the patterns, and Λ_L was varied from 500 to 680 nm in 20 nm steps. The extinction spectrum of the rectangular lattice was strongly dependent on the illuminating polarization, due to plasmonic coupling of the nanodisks periodically arranged in the two perpendicular directions. The P_S-polarized peak appeared at a longer wavelengths than the P_L-polarized one. Furthermore, by increasing the long period Λ_L, the P_S peak shifted toward longer wavelengths, while the wavelength of the P_L peak did not vary much, and the spectra of both modes broadened significantly. This behavior is opposite of what one would expect from the previously considered nanoplasmonic arrays with substantially subwavelength periods;[35] that is, for a given polarization, the extinction strength depends primarily on the spacing between the nanodisks in the orthogonal direction. In the present experiments the spacings are always on a scale of between a half and one wavelength, and the coupling between the individual nanodisks must include retardation effects. Then, it is natural that the electromagnetic mode polarized in a given

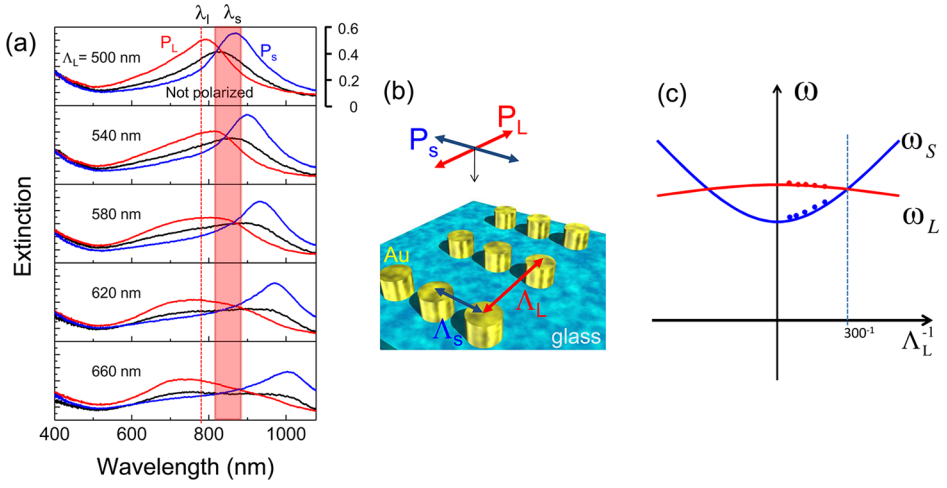

Figure 2. (a) Experimental extinction spectra of the periodic array of nanodisks under illumination by nonpolarized light (black line) and light polarized along P_S (blue) and P_L (red). The wavelengths of excitation and Raman scattering are λ_l and λ_s, respectively. (b) Schematic illustration of polarization and rectangular pattern of the nanodisks. (c) Dispersion curves of P_S and P_L modes. Calculated dispersion curves for the P_S and P_L modes; the crossover point is at square lattice Λ_L = 300 nm (dashed line).

dx.doi.org/10.1021/ph500228s | ACS Photonics 2014, 1, 1006−1012

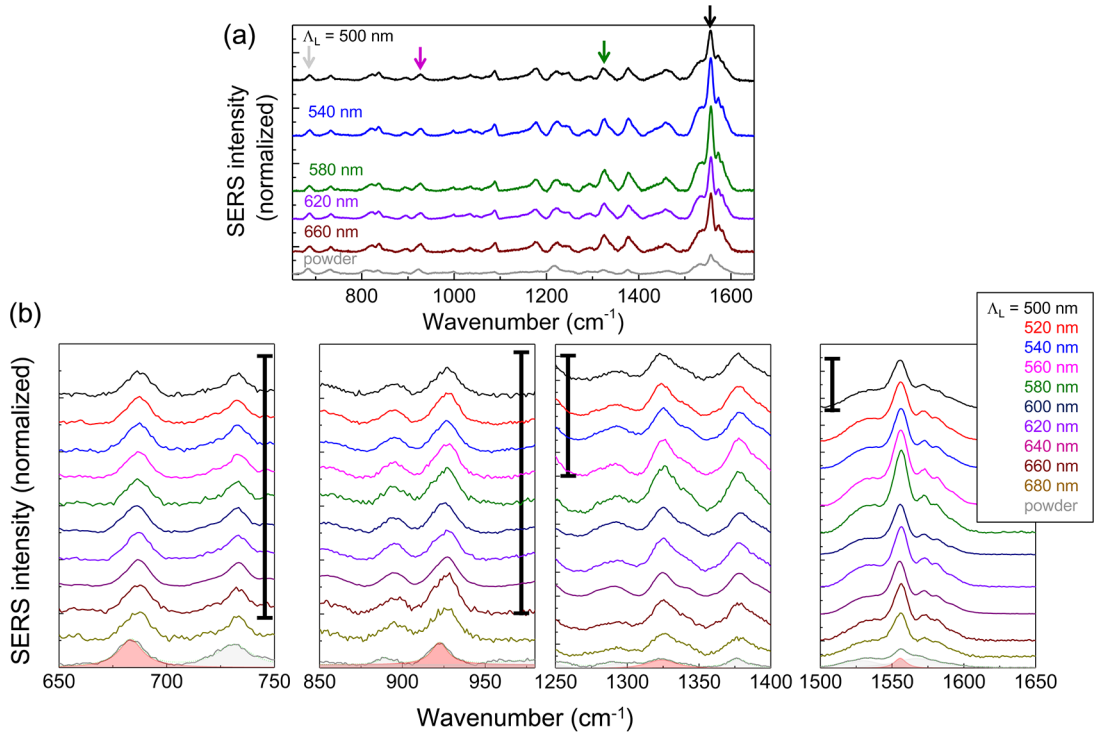

Figure 3. (a) Experimental SERS spectra of IR-26 dye adsorbed on Au nanodisks of a rectangular lattice at different values of Λ_L; Λ_S = 300 nm. The SERS peaks selected for the analysis are located at 685, 925, 1325, and 1558 cm^{-1} (λ_s = 830, 846, 876, and 894 nm for λ_l = 785 nm). (b) SERS spectra of selected peaks of 685, 925, 1325, and 1558 cm^{-1}. SERS signals were normalized by the intensity of 685 cm^{-1} of each spectra. The bars in the graphs indicate a scale of 10. The double-sided arrows indicate the intensity of SERS used for the analysis. The reference Raman scattering from the IR-26 powder is shown at the bottom of the plots with color-coded peak deconvolution.

direction can "sense" the change of periodicity in the orthogonal direction (i.e., the direction of the in-plane propagation), as shown in Figure 1.

Thus, the broad peak shown by the spectra in Figure 2a can be attributed to the plasmonic band that is created by coupling of the localized plasmon modes rather than due to diffraction, which would cause spectrally sharper resonances. This conclusion is consistent with earlier observations.[33,31,37−39] The surface modes in the plasmonic band are essentially transverse; hence the coupling is influenced by the periodicity normal to the polarization direction. The effect of Λ_L on the resonance frequency can be understood in the following way. For P_S polarization the field acting on the disks increases as Λ_L decreases (induced dipole fields are parallel); hence restoring force and resonant frequency ω_S increase with wavevector Λ_L^{-1}, as shown in the dispersion curves in Figure 2c. For P_L polarization, neighboring disks are only affected by a weak dipole−dipole near-field interaction (induced dipole fields are antiparallel); hence restoring force and resonant frequency ω_L slightly decrease with Λ_L^{-1}. The two curves naturally intersect for a square lattice condition. The relationship between periods and peak wavelengths (i.e., long wavelength for P_S and short for P_L) will be further discussed in the FDTD analysis part. It is noteworthy that the dispersion curves in Figure 2c are quadratic, typical of the tight-binding calculation of coupling, rather than linear for a diffraction Bragg condition, indicating that the coupling between neighboring disks is dominating over the far-field diffraction.

Figure 3a shows the normalized SERS spectra of the IR-26 dye absorbed on the Au nanodisks under P_S-polarized excitation. The baselines of Raman spectra have been corrected for the background caused by the glass substrates. In order to provide a fair assessment of SERS, Raman spectra of the powdered state of IR-26 were also measured and are displayed in Figure 3a. Selected SERS peaks were fitted by least-squares method with the multipeak Lorenzian functions, and an integrated area of SERS peaks was used for analysis. Each peak was normalized by the SERS intensity at 685 cm^{-1} (see Figure 3b) for discussion of SERS selectivity. With increasing Λ_L, the absolute SERS intensity decreased, due to the decrease of the area density of disks.

The SERS enhancement is proportional to the absolute value of EM field enhancement, while the extinction is related to the imaginary part of the response of the medium to the electric field, i.e., the polarizability of the medium; therefore the relationship of SERS intensity scales with extinction of plasmon resonances (SERS scaling factors) as[40]

$$\frac{\text{SERS}}{\text{Ext}_l \times \text{Ext}_R} \approx \frac{f_{\text{dye}}}{\gamma(\nu_l)\,\gamma(\nu_R)} \tag{1}$$

where f_{dye} is the Raman scattering of dye molecule integrated over the surface of nanodisks, γ is the decay constant of the nanodisks at excitation and the Raman (Stokes) frequencies, and Ext_l and Ext_R are the extinction value at the excitation laser (785 nm in this work) and extinction at the Raman Stokes wavenumber, respectively. We have determined extinction at laser wavelength Ext_l using polarized light, while for the Stokes frequency we have used the value of Ext_R for the unpolarized light because this relationship reproduces experimental conditions in which the laser light is polarized while all Raman emission is collocated independent of polarization.[40] Next, we define a SERS selectivity, Sel, as the ratio of SERS scaling factors at two peaks (eq 2):

dx.doi.org/10.1021/ph500228s | ACS Photonics 2014, 1, 1006−1012

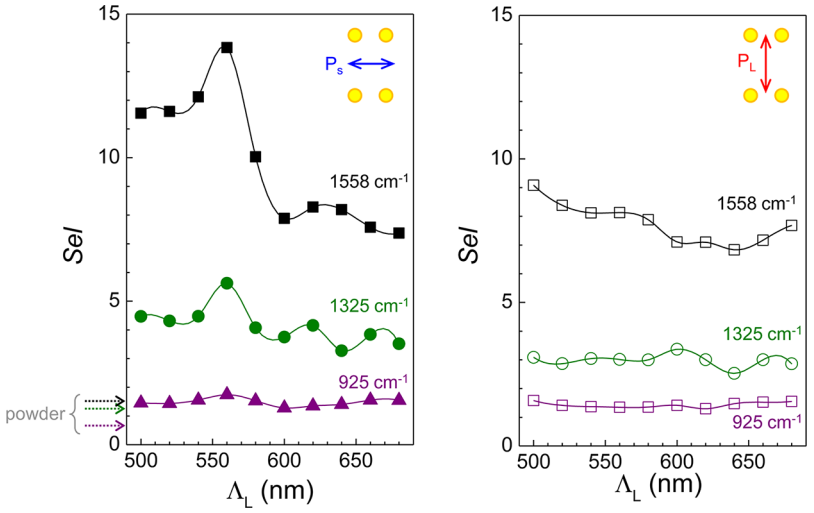

Figure 4. SERS selectivity Sel vs the Λ_L for varying SERS peak wavenumber R. The filled markers (left panel) represent the P_S polarization excitation; counter markers (right panel) indicate P_L polarization laser excitation. The dashed arrows indicate the powder Raman selectivity (which can be defined as the integration Raman area ratio, $A_R/A_{685cm^{-1}}$) obtained from the IR-26 powder.

$$\mathrm{Sel} = \frac{\mathrm{SERS}_R}{\mathrm{Ext}_l \times \mathrm{Ext}_R} \Big/ \frac{\mathrm{SERS}_{685\mathrm{cm}^{-1}}}{\mathrm{Ext}_l \times \mathrm{Ext}_{685\mathrm{cm}^{-1}}} \equiv \frac{\mathrm{SERS}_R}{\mathrm{SERS}_{685\mathrm{cm}^{-1}}} \frac{\mathrm{Ext}_{685\mathrm{cm}^{-1}}}{\mathrm{Ext}_R} \quad (2)$$

where $\mathrm{Ext}_{685\mathrm{cm}^{-1}}$ is the nonpolarized extinction at 685 cm^{-1} (R = 685 cm^{-1}). The 685 cm^{-1} mode was chosen as the reference, since it is the closest to the Rayleigh laser line. We have chosen the R = 925, 1325, and 1558 cm^{-1} modes (Figure 3); the observed trends are applicable to the other peaks also. The value of Sel changes with Λ_L and depends on the polarization of the exciting light, as discussed next.

As shown in Figure 4, the SERS selectivity Sel increases with separation from Λ_L = 500 to 580 nm, when the resonance wavelength of the P_S mode moved closer to the Stokes wavelength. It is especially apparent when compared with the selectivity under excitation polarized along P_L. For spacings larger than 600 nm, the selectivity Sel dropped to almost the same values as observed for the P_L mode. This trend could also be seen for the 1325 cm^{-1} mode. Close to the excitation laser wavelength (smaller wavenumbers), SERS intensities of the P_S and P_L modes are the same within the margin of error (see the 925 cm^{-1} peak). This indicates that the SERS signal scales with extinction of the P_S mode and can be tuned to enhance selectivity. SERS selectivity increases in comparison with selectivity of the dye powder, which can be attributed to the molecular orientation at the surface (a chemical effect).

A beneficial increase in selectivity obtained by varying the lattice spacing has been accompanied by a deleterious reduction in absolute intensity caused by the reduced surface density of the nanodisks. To compensate for this decline in absolute intensity, one should look for additional means of SERS enhancement. We previously reported the randomization of patterns as one of the solutions to increase the SERS intensity.[34] However, randomization causes reduction of selectivity. We discuss next the trade-off between randomization and selectivity for SERS intensity enhancement using randomization.

Figure 5 shows the gradual variation of the extinction spectra in the spectral window of 400−1060 nm due to randomization and the corresponding SEM images of the patterns. We start

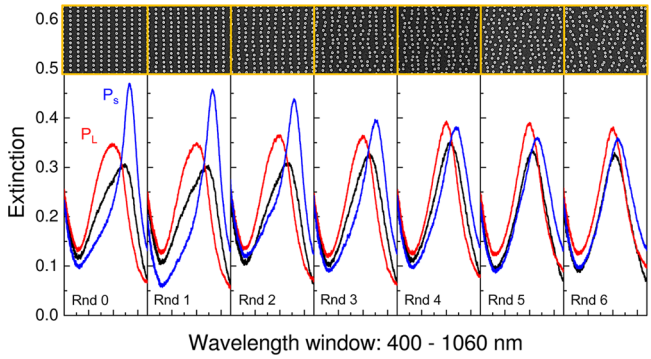

Figure 5. Experimental extinction spectra for increasing randomness (Rnd), and SEM images of the corresponding patterns (top row). The pitch of the pattern defines a cell 300 × 580 nm^2.

from the 300 × 580 nm^2 lattice, because this pattern has a strong selectivity dependence on extinction (Figure 4). For increasing randomization, the extinction maxima of the P_L and P_S modes close in on one another. The randomness factor is defined as Rnd = 0 to 6, where 0 corresponds to the periodic pattern, and the maximum random walking distances from periodic patterns in the x- (pitch Λ_S) and y-directions (pitch Λ_L) are defined by Δx = Rnd × Λ_S/6 and Δy = Rnd × Λ_L/6, respectively. As shown in Figure 5, the sample with Rnd = 6 is still not fully randomized, as its extinction spectra have a slight polarization dependence on the P_L and P_S modes.

The SERS selectivity Sel and SERS scaling factor (SERS/($\mathrm{Ext}_l \times \mathrm{Ext}_R$)) (SERS intensity is normalized by the extinction factors at the excitation and scattering wavelengths ($\mathrm{Ext}_l \times \mathrm{Ext}_R$)), as a function of randomness Rnd, are shown in Figure 6, where the pattern of the highest selectivity, Λ_L = 580 nm, is presented. The selectivity decreased with increasing randomization as expected (Figure 6a), especially for the 1558 cm^{-1} mode. As the randomness reached Rnd ≈ 5, there were no recognizable differences any more between P_L and P_S excitation. However, the relative SERS intensity around Rnd = 2−3 is already about 2 times higher as compared to that of a periodic pattern. This behavior of SERS intensity with randomization has been explained previously:[36] increasing randomness favors

dx.doi.org/10.1021/ph500228s | ACS Photonics 2014, 1, 1006−1012

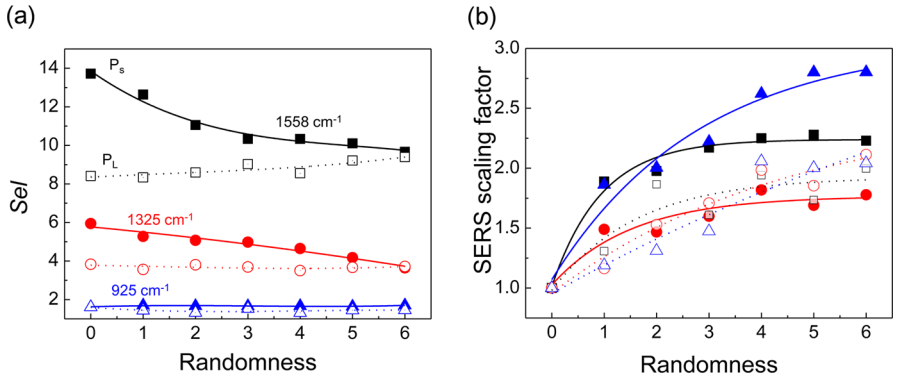

Figure 6. (a) Selectivity Sel dependence on the randomness Rnd. (b) Relative SERS intensity normalized by the extinction factors $Ext_I \times Ext_R$ vs randomness Rnd.

theh creation of "hot-spots", in which a disproportionately high field concentration occurs, causing an increase in the SERS intensity. Therefore, from Rnd = 0 to 4 there is a trade-off relationship between reasonable selectivity Sel and augmented SERS intensity. When we thought about the actual signal of SERS (meaning without normalization by extinction factors), SERS intensities were improved (1.5−3.6 times), appearing at Rnd = 3 in all selected SERS modes.

The layouts for randomness Rnd = 0, 3, and 6 were simulated by the 3D-FDTD method using the Lumerical software, according to the procedure previously outlined,[36] applied to a 10 × 10 array of nanodisks (3.3 × 6.4 μm^2 region with the same layout as used in electron beam lithography). Figure 7 shows the calculated intensity distributions in the

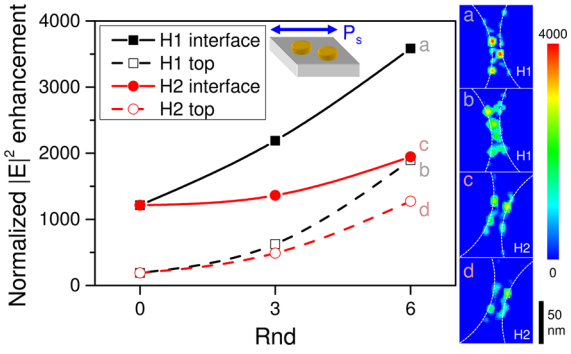

Figure 7. *E*-field intensity $|E|^2$ linear scale enhancement at wavenumber 1558 cm^{-1}, for P_S polarization at a glass interface and on top of gold nanodisks, for the two main hot-spots (H1 and H2) found in the Rnd = 6 layout, and variation for changing randomness Rnd = 0, 3, 6. The insets depict the field intensity distributions in the hot-spot regions for Rnd = 6; the white dotted lines show the nanodisk geometry.

neighborhoods of the two strongest hot-spots (named H1 and H2) found in the layout for maximum randomness Rnd = 6. Such hot-spots, having a peak intensity at the interface between gold and glass, are responsible for the 3−4 times increased SERS intensity observed in experiments and occur preferentially in the narrow gaps formed when two nanodisks are brought close to each other by the random walk. The enhancements obtained for P_S polarization are shown, as they are significantly stronger than those for P_L polarization, due to the shorter average distance between the particles along the *x*-axis. Several random walk designs were tested numerically and resulted in the qualitatively same result in terms of field enhancement and extinction spectrum.

The evolution of increasing randomness shows a steady increase in the localized enhancement of 1.5−3 times at the interface between nanodisks and the glass, where the field is strongest, and up to 10 times at the top corner of the nanodisk, where the enhancement is low in the regular lattice. The steady increase continues into the randomness range, where SERS shows a saturation in Figure 6b, as the simulated enhancement is taken at a specific location on the sample, while the measurement is averaged over all the surface. The model also shows how the random alignment of the nanodisks permits the plasmonic modes to harvest energy from one polarization while distributing the scattering also on the perpendicular one, according to the direction of the dipole mode axis. Moreover, the extinction cross-section was also calculated by the same numerical procedure, to confirm the trend and dependence on P_S and P_L shown in Figure 5. The results are shown in Figure 8,

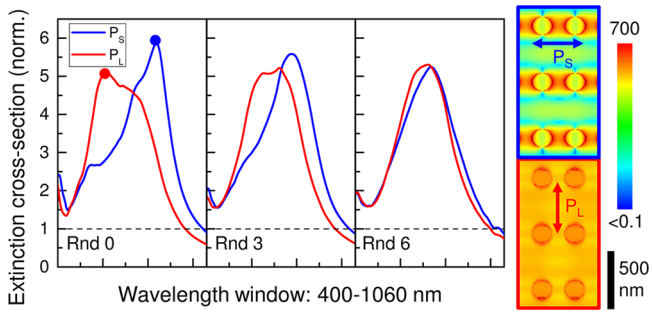

Figure 8. Calculated extinction cross-section for increasing randomness Rnd = 0, 3, and 6 using the same layouts as in Figure 5, confirming the trend and dependence on P_S and P_L. The cross-section is calculated by averaging on a cluster of 20 nanodisks and normalized to the geometrical area of the cluster, indicated by the black dashed line. The glass interface *E*-field intensity $|E|^2$ log-scale plots at the maximum extinction wavelengths (Rnd = 0, right side) show a maximum enhancement of 700 for P_S and 350 for P_L.

where the cross-section is calculated by taking a cluster of 20 nanodisks at the specific degree of randomness as an average for the whole region and normalizing the cross-section to the geometrical area of the gold in the cluster. The comparison with the experimental results reveals how the plasmonic resonance boosts extinction up to 6 times with respect to the same area of gold. The less smooth behavior of the curves is an effect of the limited number of nanodisks on average, and the

dx.doi.org/10.1021/ph500228s | *ACS Photonics* 2014, 1, 1006−1012

wavelength shift with respect to the experiment is an effect of the slight shape differences between the fabricated and simulated arrays.

In the P_S case, the pitch is smaller than the critical value for radiation, but the phase retardation between neighboring disks is such that the scattered field still propagates almost in-phase with the exciting light wave, which increases the localized field. The energy of the mode is strongly localized on the nanodisks (one can think of an analogy with the tight binding mode in the solid state, where the electrons move but their energy is highest near the ions). The resulting depolarization affects the induced dipole moment of the single nanodisk, leading to a red-shift of the extinction peak.[41] This is confirmed by the glass interface E-field intensity $|E|^2$ enhancement plots (Rnd = 0) in Figure 8, which show twice as high enhancement for the P_S case (700 vs 350) and a stronger field localization. As described earlier, the near-field coupling between disks governs extinction, as explicitly shown in Figure 2c.

CONCLUSIONS

In this study, we demonstrated SERS selectivity control on rectangular lattice patterns of nanodisks. The SERS selectivity is strongly related to the extinction resonance at the Raman scattering wavelength. Also, we demonstrated the effect of randomization on SERS intensity in rectangular lattices. At small disorder levels, with randomization level from Rnd = 0 up to a half-period long random walk, the SERS intensity can be increased by a factor of 2 at the cost of reduced selectivity. This randomization strategy for control of SERS intensity and spectral selectivity can be used together with the back-side illumination geometry in SERS, which provides an extra enhancement due to a favorable phase matching of the transmitted and reflected beams in the case of back-side illumination; it is accounted for in the Fresnel coefficients for the E-field amplitudes.[42]

It is shown that a significant change in extinction at a certain wavelength for one polarization can be created by the presence of light at the same wavelength but at a perpendicular polarization. This coupling between two perpendicular polarizations can open new applications in SERS via an all-optical control of light scattering and absorption of the pump beam by polarization of the probe (at the same or slightly different wavelength within an extinction peak). All-optical diffraction control by coupling of two orthogonally polarized beams using geometrically coupled plasmonic nanoparticles has been recently demonstrated.[43] All-optical ultrafast switching is one of the inherent features of plasmonics that is promising for practical applications in data communications where Tbits/s speeds are required.

AUTHOR INFORMATION

Corresponding Author

*E-mail: nishijima@ynu.ac.jp.

Notes

The authors declare no competing financial interest.

ACKNOWLEDGMENTS

Y.N. gratefully thanks Prof. Toshihiko Baba from Yokohama National University for fruitful discussions and for granting access to fabrication and characterization facilities. This work was financially supported by the Research Foundation for Opt-Science and Technology. S.J. is grateful for support via the Australian Research Council DP130101205 project. Part of this work was performed on the swinSTAR supercomputer at Swinburne University of Technology.

REFERENCES

(1) Fleischmann, M.; Hendra, P. J.; McQuillan, A. J. Raman spectra of pyridine adsorbed at a silver electrode. *Chem. Phys. Lett.* **1973**, *26*, 163−166.

(2) Moskovits, M. Surface-enhanced Raman spectroscopy: a brief retrospective. *J. Raman Spectrosc.* **2005**, *36*, 485−496.

(3) Camden, J. P.; Dieringer, J. A.; Zhao, J.; Van Duyne, R. P. Controlled plasmonic nanostructures for surface-enhanced spectroscopy and sensing. *Acc. Chem. Res.* **2008**, *41*, 1653−1661.

(4) Talley, C. E.; Jackson, J. B.; Oubre, C.; Grady, N. K.; Hollars, C. W.; Lane, S. M.; Huser, T. R.; Nordlander, P.; Halas, N. J. Letter surface-enhanced raman scattering from individual Au nanoparticles and nanoparticle dimer substrates. *Nano Lett.* **2005**, *5*, 1569−1574.

(5) Genov, D. A.; Sarychev, A. K.; Shalaev, V. M.; Wei, A. Resonant field enhancements from metal nanoparticle arrays. *Nano Lett.* **2004**, *4*, 153−158.

(6) Xu, H. X.; Aizpurua, J.; Käll, M.; Apell, P. Electromagnetic contributions to single-molecule sensitivity in surface-enhanced Raman scattering. *Phys. Rev. E* **2000**, *62*, 4318−4324.

(7) Zachariah, E.; Bankapur, A.; Santhosh, C.; Valiathan, M.; Mathur, D. Probing oxidative stress in single erythrocytes with Raman tweezers. *J. Photochem. Photobiol. B: Biol.* **2010**, *100*, 113−116.

(8) Hobro, A. J.; Konishi, A.; Coban, C.; Smith, N. I. Raman spectroscopic analysis of malaria disease progression via blood and plasma samples. *Analyst* **2013**, DOI: 10.1039/C3AN00255A.

(9) Kho, K. W.; Fu, C. Y.; Dinish, U. S.; Olivo, M. Clinical SERS: are we there yet? *J. Biophotonics* **2011**, *4*, 667−684.

(10) Nishijima, Y.; Nigorinuma, H.; Rosa, L.; Juodkazis, S. Selective enhancement of infrared absorption with metal hole arrays. *Opt. Mater. Express* **2012**, *2*, 1367−1377.

(11) Nishijima, Y.; Adachi, Y.; Rosa, L.; Juodkazis, S. Augmented sensitivity of an IR-absorption gas sensor employing a metal hole array. *Opt. Mater. Express* **2013**, *3*, 968−976.

(12) Dasary, S. S. R.; Singh, A. K.; Senapati, D.; Yu, H.; Ray, P. C. Gold nanoparticle based label-free SERS probe for ultrasensitive and selective detection of trinitrotoluene. *J. Am. Chem. Soc.* **2009**, *131*, 13806−13812.

(13) Senapati, T.; Senapati, D.; Singh, A. K.; Fan, Z.; Kanchanapally, R.; Ray, P. C. Highly selective SERS probe for Hg(II) detection using tryptophan-protected popcorn shaped gold nanoparticles. *Chem. Commun.* **2011**, *47*, 10326−10328.

(14) Kneipp, J.; Kneipp, H.; Rice, W. L.; Kneipp, K. Optical probes for biological applications based on surface-enhanced Raman scattering from indocyanine green on gold nanoparticles. *Anal. Chem.* **2005**, *77*, 2381−2385.

(15) Alexander, T. A.; Le, D. M. Characterization of a commercialized SERS-active substrate and its application to the identification of intact Bacillus endospores. *Appl. Opt.* **2007**, *46*, 3878−3890.

(16) Wang, Y.; Yan, B.; Chen, L. SERS tags: novel optical nanoprobes for bioanalysis. *Chem. Rev.* **2013**, *113*, 1391−1428.

(17) Tripp, R. A.; Dluhy, R. A.; Zhao, Y. Novel nanostructures for SERS biosensing. *Nanotoday* **2008**, *3*, 31−37.

(18) Xu, B. B.; Zhang, R.; Liu, X. Q.; Wang, H.; Zhang, Y. L.; Jiang, H. B.; Wang, L.; Ma, Z. C.; Ku, J. F.; Xiao, F. S.; Sun, H. B. On-chip fabrication of silver microflower arrays as a catalytic microreactor for allowing in situ SERS monitoring. *Chem. Commun.* **2012**, *48*, 1680−1682.

(19) Kowalska, E.; Janczarek, M.; Rosa, L.; Juodkazis, S.; Ohtani, B. Mono- and bi-metallic plasmonic photocatalysts for degradation of organic compounds under UV and visible light irradiation. *Catal. Today* **2013**, corrected proof, available online Dec 7, 2013.

(20) Lee, M.; Lee, K.; Kim, K. H.; Oh, K. W.; Choo, J. SERS-based immunoassay using a gold array-embedded gradient microfluidic chip. *Lab Chip* **2012**, *12*, 3720−3727.
(21) Xu, B. B.; Ma, Z. C.; Wang, H.; Liu, X. Q.; Zhang, Y. L.; Zhang, X. L.; Zhang, R.; Jiang, H. B.; Sun, H. B. A SERS-active microfluidic device with tunable surface plasmon resonances. *Electrophoresis* **2011**, *32*, 3378−3384.
(22) Xu, B. B.; Zhang, Y. L.; Xia, H.; Dong, W. F.; Dingc, H.; Sun, H. B. Fabrication and multifunction integration of microfluidic chips by femtosecond laser direct writing. *Lab Chip* **2013**, *13*, 1677−1690.
(23) Le Ru, E. C.; Galloway, C.; Etchegoin, P. G. On the connection between optical absorption/extinction and SERS enhancements. *Phys. Chem. Chem. Phys.* **2006**, *8*, 3083−3087.
(24) Grand, J.; Kostcheev, S.; Bijeon, J.-L.; Lamy de la Chapelle, M.; Adam, P. M.; Rumyantseva, A.; Lérondel, G.; Royer, P. Optimization of SERS-active substrates for near-field Raman spectroscopy. *Synt. Met.* **2003**, *139*, 621−624.
(25) Le Ru, E. C.; Grand, J.; Félidj, N.; Aubard, J.; Lévi, G.; Hohenau, A.; Krenn, J. R.; Blackie, E.; Etchegoin, P. G. Experimental verification of the SERS electromagnetic model beyond the $|E|^4$ approximation: polarization effects. *J. Phys. Chem. C* **2008**, *112*, 8117−8121.
(26) Marimuthu, A.; Christopher, P.; Linic, S. Design of plasmonic platforms for selective molecular sensing based on surface-enhanced raman spectroscopy. *J. Phys. Chem. C* **2012**, *116*, 9824−9829.
(27) Lassiter, J. B.; Sobhani, H.; Fan, J. A.; Kundu, J.; F. Capasso, P. N.; Halas, N. J. Fano resonances in plasmonic nanoclusters: geometrical and chemical tunability. *Nano Lett.* **2010**, *10*, 3184−3189.
(28) Hao, F.; Sonnefraud, Y.; Dorpe, P. V.; Maier, S. A.; Halas, N. J.; Nordlander, P. Symmetry breaking in plasmonic nanocavities: subradiant LSPR sensing and a tunable Fano resonance. *Nano Lett.* **2008**, *8*, 3983−3988.
(29) Sonnefraud, Y.; Verellen, N.; Sobhani, H.; Vandenbosch, G. A.; Moshchalkov, V. V.; Dorpe, P. V.; Nordlander, P.; Maier, S. A. Experimental realization of subradiant, superradiant, and Fano resonances in ring/disk plasmonic nanocavities. *ACS Nano* **2008**, *4*, 1664−1670.
(30) Herzog, J. B.; Knight, M. W.; Li, Y.; Evans, K. M.; Halas, N. J.; Natelson, D. Dark plasmons in hot spot generation and polarization in interelectrode nanoscale junctions. *Nano Lett.* **2013**, *13*, 1359−1364.
(31) Auguie, B.; Barnes, W. L. Collective resonances in gold nanoparticles arrays. *Phys. Rev. Lett.* **2008**, *101*, 143902.
(32) Kravets, V. G.; Schedin, F.; Grigorenko, A. N. Extremely narrow plasmon resonances based on diffraction coupling of localized plasmons in arrays of metallic nanoparticles. *Phys. Rev. Lett.* **2008**, *101*, 087403.
(33) Rahmani, M.; Miroshnichenko, A. E.; Lei, D.; Luk'yanchuk, B.; Kuznetsov, M. I. T. A. I.; Kivshar, Y. S.; Francescato, Y.; Giannini, V.; Hong, M.; Maier, S. A. Beyond the hybridization effects in plasmonic nanoclusters: diffraction-induced enhanced absorption and scattering. *Small* **2014**, *10*, 576−583.
(34) Nishijima, Y.; Rosa, L.; Juodkazis, S. Surface plasmon resonances in periodic and random patterns of gold nano-disks for broadband light harvesting. *Opt. Express* **2012**, *20*, 11466−11477.
(35) Khurgin, J. B.; Sun, G. Impact of disorder on surface plasmons in two-dimensional arrays of metal nanoparticles. *Appl. Phys. Lett.* **2009**, *94*, 221111.
(36) Nishijima, Y.; Khurgin, J. B.; Rosa, L.; Fujiwara, H.; Juodkazis, S. Randomization of gold nano-brick arrays: a tool for SERS enhancement. *Opt. Express* **2013**, *21*, 13502−13514.
(37) Kuznetsov, A. I.; Evlyukhin, A. B.; Gonçalves, M. R.; Reinhardt, C.; Koroleva, A.; Arnedillo, M. L.; Kiyan, R.; Marti, O.; Chichkov, B. N. Laser fabrication of large-scale nanoparticle arrays for sensing applications. *ACS Nano* **2011**, *5*, 4843−4849.
(38) Bi, Y.-G.; Feng, J.; Li, Y.-F.; Zhang, X.-L.; Liu, Y.-F.; Jin, Y.; Sun, H.-B. Broadband light extraction from white organic light-emitting devices by employing corrugated metallic electrodes with dual periodicity. *Adv. Mater.* **2013**, *25*, 6969−6974.
(39) D'Aguanno, G.; Mattiucci, N.; Bloemer, M. J.; de Ceglia, D.; Vincenti, M. A.; Alù, A. Transmission resonances in plasmonic metallic gratings. *J. Opt. Soc. Am. B* **2011**, *28*, 253−264.
(40) Nishijima, Y.; Hashimoto, Y.; Rosa, L.; Khurgin, J. B.; Juodkazis, S. Scaling of rules of SERS intensity. *Adv. Opt. Mater.* **2014**, *2*, 382−388.
(41) Meier, M.; Wokaun, A.; Liao, P. F. Enhanced fields on rough surfaces: dipolar interactions among particles of sizes exceeding the Rayleigh limit. *J. Opt. Soc. Am. B* **1985**, *2*, 931−949.
(42) Jayawardhana, S.; Rosa, L.; Juodkazis, S.; Stoddart, P. R. Additional enhancement of electric field in surface-enhanced Raman scattering due to Fresnel mechanism. *Sci. Rep.* **2013**, *3*, 2335.
(43) Davis, T. J.; Gómez, D. E.; Eftekhari, F. All-optical modulation and switching by a metamaterial of plasmonic circuits. *Opt. Lett.* **2014**, *39*, 4938−4941.